Theor Chem Acc (2011) 129:757–769
DOI 10.1007/s00214-011-0933-9

REGULAR ARTICLE

Activation of carboplatin by chloride ions: a theoretical investigation

Antonella Ciancetta · Cecilia Coletti · Alessandro Marrone · Nazzareno Re

Received: 2 December 2010 / Accepted: 28 March 2011 / Published online: 30 April 2011

Abstract We carried out a theoretical study to investigate the thermodynamics and the kinetics of the reaction of the anticancer drug carboplatin with chloride ions, of potential interest to clarify the in vivo mechanism of action of this compound. The reaction consists of two consecutive substitution steps that lead to the removal of the malonate moiety and the formation of cisplatin. Because the acidity of the solution seems to play an important role on the actual outcome and rate of the reaction, different pH conditions (corresponding to neutral, weakly acidic, and strongly acidic environments) have been investigated, by considering differently protonated species. Our results are in good agreement with the few experimental evidences, indicating that the process is very unlikely to occur in neutral or weak acidic media, whereas a concentrated acidic environment leads to the fast and irreversible conversion of carboplatin to cisplatin.

Keywords Carboplatin · Activation · Chloride anion · DFT · MP2

1 Introduction

Cisplatin, cis-diamminedichloro-platinum(II) or [$(NH_3)_2PtCl_2$], is one of the most widely used antitumor drugs and is most active against a variety of tumors, especially testicular and ovarian cancers [1–3]. However, its clinical success is limited by severe side effects which have led to the development of second-generation platinum compounds with improved pharmacological properties such as carboplatin, cis-diammine(cyclo-butane-1,1-dicarboxylato)-platinum(II) or [$(NH_3)_2Pt(CBDCA)$], and oxaliplatin, (1R,2R-diaminocyclohexane)oxalato-platinum(II) or [$(DACH)PtCl_2$] [4]. Among them, carboplatin is currently used in the clinical treatment of cancer with about the same spectrum of activity of cisplatin but with reduced toxicity [5]. The mechanism of action of cisplatin has been widely investigated and is relatively well established at least in the first stages: It enters cells mainly by passive diffusion and then undergoes hydrolysis in vivo to the active species $[Pt(NH_3)_2Cl(OH_2)]^+$ and $[Pt(NH_3)_2(OH_2)_2]^{2+}$ which subsequently bind to DNA causing a distortion of the helical structure and with consequent inhibition of DNA replication and transcription [2]. On the other hand, the mode of action of carboplatin has been much less studied and is not yet fully clarified [5]. Both cisplatin and carboplatin have two stable *cis* ammino ligands, whereas the two labile chloro ligands of cisplatin are replaced by a dicarboxylate chelate ring in carboplatin. The close analogy between the two compounds suggests a similar mode of action and, indeed, for carboplatin it has been shown that $Pt(NH_3)_2^{2+}$ binds to DNA in vivo [5]. However, the bidentate malonate ring is more difficult to replace in substitution reactions than the chloride ions and thus carboplatin is much less reactive than cisplatin. At neutral pH at 37 °C, the rate constant for the first aquation reaction of carboplatin is very small, $k_1 \approx 10^{-8}$–10^{-7} s^{-1}, 2–3 orders of magnitude smaller than the constant for cisplatin, $k_1 \approx 10^{-4}$ s^{-1}, likely ruling out aquation as a means of activation of this drug in vivo. Moreover, as the aquated Pt(II) species are

Electronic supplementary material The online version of this article (doi:10.1007/s00214-011-0933-9) contains supplementary material, which is available to authorized users.

A. Ciancetta · C. Coletti · A. Marrone · N. Re (✉)
Dipartimento di Scienze del Farmaco, Università degli Studi "G. D'Annunzio" Chieti-Pescara, Via dei Vestini, 66100 Chieti, Italy
e-mail: nre@unich.it

produced more slowly and probably in a different form from cisplatin, the binding mode of carboplatin to DNA could significantly change [4]. In view of this inertness of carboplatin toward aquation, several suggestions have been made to account for its activity in vivo, such as the displacement of the malonate ring by Cl^- ions or by sulfur nucleophiles such as cysteine or methionine surface residues of proteins, or the glutathione molecule, present in blood plasma [2, 8]. In particular, the rate of hydrolysis of carboplatin, and hence the interaction with DNA, has been shown to be increased in the presence of various nucleophiles [6, 7, 9]. The reaction of carboplatin with chloride has been investigated in detail, because of the significant chloride ion concentration in blood plasma and also because the effectiveness of carboplatin is known to be increased by first incubating it in sodium chloride solution [10]. Several experimental studies have addressed the kinetics of the reaction of carboplatin with Cl^-: at 25 and 80 °C at various pH values [6], between 43 and 70 °C again with varying pH [9], and at physiological conditions (37 °C and pH = 7) [7]. All these studies showed that the reaction may occur, at least at the highest considered temperatures, leading to cisplatin and suggesting that, in the presence of chloride ions, the carboplatin could in principle behave as a prodrug leading to cisplatin which, in those conditions, may easily hydrolyze.

Kinetic studies have pointed out an acid-catalyzed mechanism for carboplatin aquation, involving the protonation of the carbonyl oxygen atoms of the malonate ring [11], and indeed the above mentioned studies have shown that the kinetics of carboplatin activation by Cl^- is also affected by the pH of the solution. A deeper insight into the carboplatin activation and its dependence on the pH is therefore important to understand its mechanism of action in vivo and may be useful to design new platinum-based anticancer drugs. To this end, we carried out DFT and local MP2 calculations to investigate the thermodynamics and the kinetics of the substitution of the malonate ring in carboplatin by Cl^- in both neutral and acidic conditions, see Scheme 1. Although several theoretical investigations

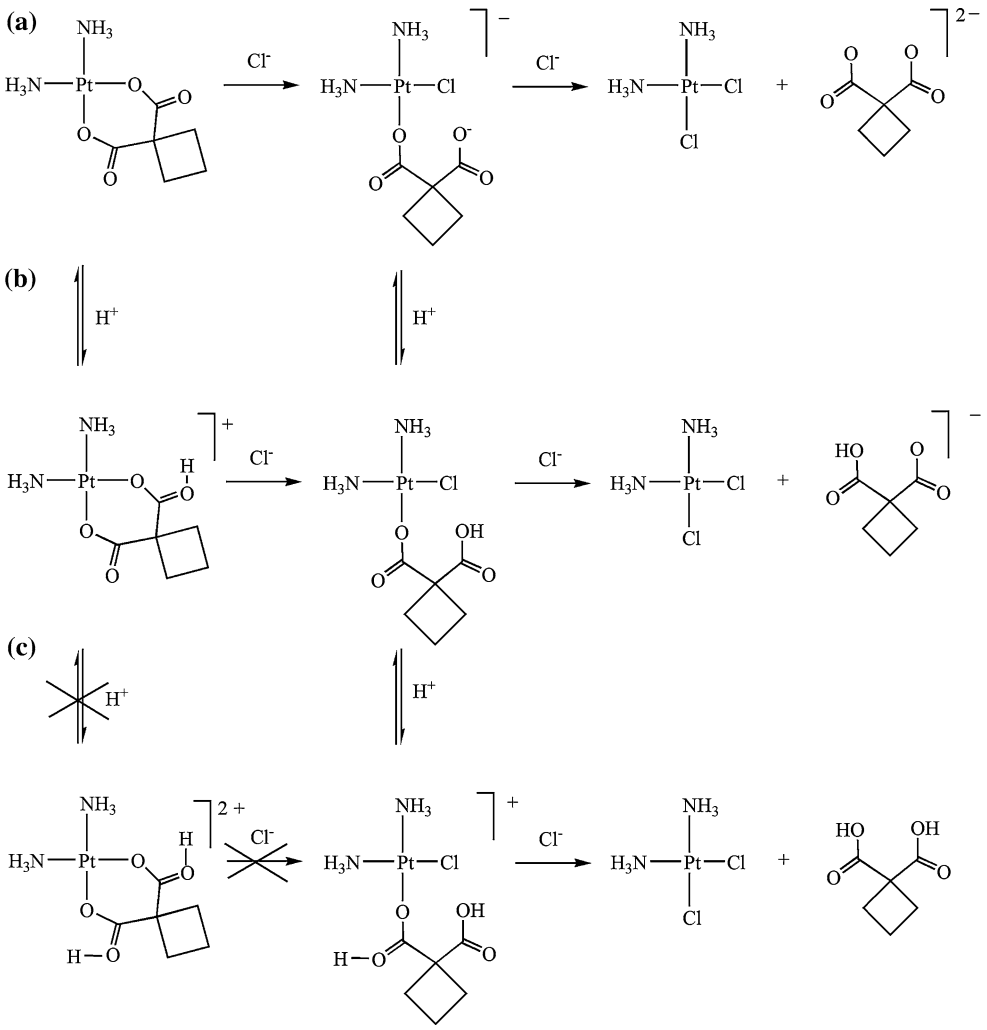

Scheme 1 Possible paths for the activation of carboplatin with differently protonated species, corresponding to various pH conditions

have addressed the aquation of cisplatin [12] and of the second-generation platinum antitumor complexes [13–16], to the best of our knowledge, only one theoretical study has been very recently performed on the Cl^- activation of this class of compounds, but limited to oxaliplatin [16].

2 Computational details

All calculations were made with the Jaguar 7.5 quantum chemistry package [17] using density functional theory (DFT) with the B3LYP hybrid functional [18, 19], which is known to give a good description of reaction profiles for transition metal-containing compounds [20, 21] and the local Møller-Plesset (LMP2) approximation [22]. The 1s-4d core electrons of the platinum atom were described with the Hay and Wadt core-valence relativistic (i.e., with an implicit treatment of scalar-relativistic effects) effective core-potential (ECP) leaving the outer 18 electrons to be treated explicitly by a basis set of double-ζ quality [23], whereas all electrons were considered for the remaining atoms with the 6-31G** basis set (denoted as LACVP** in Jaguar [24]). All minima and transition state structures were optimized in gas phase with this basis set and the B3LYP functional. Frequency calculations were made to verify the correct nature of the stationary points and to estimate zero-point energy (ZPE) and thermal corrections to thermodynamic properties. Intrinsic reaction coordinate (IRC) calculations were employed to correctly locate reagents and products minima connected with the transition states for each considered reaction step. Test calculations were also made using the M06 functional [25], recently introduced to take into account some of the possible limitations [26, 27] of older functionals. Geometries obtained by optimizing with this functional for the first activation step in neutral medium (see next section, Fig. 1 and Table S1 in Supporting Information) are very close to those obtained with B3LYP.

All structures were reoptimized in solution using the Poisson-Boltzmann (PB) continuum solvent method implemented in Jaguar, representing the solvent as a layer of charges at the molecular surface (i.e., the contact surface between the van der Waals envelope of the solute and a probe solvent molecule), serving as a dielectric continuum boundary, thus accounting for detailed molecular shape [28]. Single-point energies of all stationary points have been evaluated with a larger basis set *aug*-cc-pVTZ(-f) (i.e., without f functions) [29] for the main group elements and LACV3P+* consisting of Hay and Wadt core-valence ECP basis set of triple-ζ quality plus one diffuse d function for the metal atom. The same basis set (hereafter indicated as BS2) was also employed to compute single-point energies at LMP2 level of theory, in order to have more accurate values of reaction energies and especially of energy barriers [30, 31]. Indeed, test calculations performed by optimizing at the LMP2/BS1 level of theory on carboplatin and for the structures involved in the first activation step in neutral medium (see next section, Fig. 1 and Table S1 in Supporting Information) show geometries very close to those obtained at the B3LYP/LACVP** level of theory.

Thermodynamical properties in solution were calculated as follows. Solvation free energies were taken as the difference between the solution energies and the gas phase energies. The calculation of solvation entropies is a somewhat more delicate issue, particularly important when entropies (and free energies) need to be evaluated for bimolecular reactions involving separated reactants and products. Indeed in this case, the translational degree of freedom in the reactants/products becomes a loose

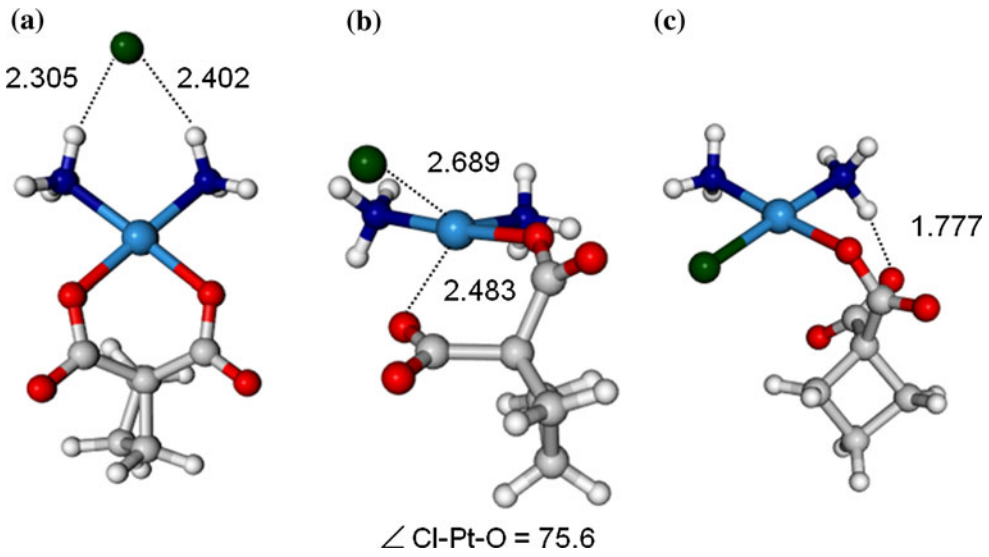

Fig. 1 Optimized geometries of the reactant adduct, RA1 (**a**), transition state, TS1, (**b**) and product adduct, PA1, (**c**) for the first activation step in neutral medium

vibration for adducts or transition states, leading to a loss/gain of entropy, much larger in the gas phase than in the confined condensed phase. For this reason, the use of gas phase entropies in solution often leads to artificially too large results. A way to overcome this problem was proposed by Werz [32] and proved to lead to solution entropies and free energies in excellent agreement with experimental values [33–37] for, among others, S_N2 substitution reactions of square planar Pt(II) complexes [33, 34]. Following this approach, a solute dissolved in a solvent loses a constant fraction of its entropy in vacuo. This loss, for water, amounts to [32, 33]:

$$\Delta S_{solvation} = -0.46\,(S^\circ - 14.3)\ \text{cal mol}^{-1}\text{K}^{-1} - 6.32\ \text{cal mol}^{-1}\text{K}^{-1}$$

which, for a qualitative estimate, is often approximated as 50% of the gas phase entropy changed of sign.

Absolute pK_a's for the mono and diprotonated carboplatin species were calculated using the equation:

$$pK_a = -\frac{\Delta G_{aq}}{2.303RT} \quad (1)$$

where ΔG_{aq} is the free energy change in solution for the considered deprotonation process and calculated as reported in Supporting Information.

3 Results and discussion

A preliminary investigation into the isolated carboplatin complex has shown that at the selected level of theory, the minimized structure matches the crystallographic data [38, 39] accurately with bond distances within 0.05 Å (with the exception of Pt–N distance, which is however within 0.1 Å) and bond angles within 10°, thus indicating that the B3LYP functional provides a good description of the molecular structures of these systems (see Supporting Information, Table S1). Moreover, comparison with the carboplatin geometries obtained optimizing with the M06 functional and the LMP2 method (also reported in Table S1) shows that they are very close, with differences in distances within 0.02 Å and in angles of, at most, 2°.

The carboplatin activation is a two-step process consisting of the stepwise substitution of the malonate moieties from platinum coordination by the sequential attack of two chloride ions: The first step involves the malonate ring opening and the second the malonate release (Scheme 1). The reaction was investigated taking into account that reagents (products) can form stable non-covalent adducts prior (after) the reaction. We have thus optimized the geometries of the reactant (RA) and product (PA) adduct intermediates, and their energies with respect to the isolated species have been evaluated and given below. The reaction and activation enthalpies and free energies have been calculated relatively to these adducts, only when they are lower than reagents infinitely apart.

Because the outcome of the reaction and its rate critically depend on the reaction conditions, we have investigated the thermodynamics and the kinetics of both steps in neutral (Scheme 1a) and in acidic medium, considering that the reacting and/or the intermediate species can be singly (Scheme 1b) or doubly (Scheme 1c) protonated under such conditions. The solvent effect has also been thoroughly addressed both by performing single-point calculations over gas phase optimized geometry and by optimizing directly in water solvent.

3.1 Activation in neutral conditions

3.1.1 Geometry structures

As mentioned above, optimizations have been performed both in gas phase and in solution, and because geometrical parameters are very close (adducts in solution are slightly looser, with intermolecular distances correspondingly longer), only the geometries in solution will be discussed.

The first activation step consists of the replacement of one carboxylate group of the malonate ligand by a chloride ion. The optimized reactant adduct RA1 geometry (Fig. 1a) for this step shows the attacking chloride ion bridging, via hydrogen bonds, the ammino ligands with Cl–H distances of 2.305 and 2.402 Å. The chloride ion is still farther from the metal center with a Pt–Cl distance of 4.237 Å, while the Pt–O(leaving) bond is almost unperturbed, 2.040 Å.

The corresponding transition state structure, TS1 (Fig. 1b, with an imaginary frequency of $-116.8\ \text{cm}^{-1}$), shows that the entering chloride has approached the metal center, whereas the oxygen of the adjacent leaving carboxylate group has moved further, with Pt–Cl and Pt–O(malonate) distances of 2.689 and 2.483 Å, respectively. An approximatively trigonal bipyramidal geometry is observed with an acute leaving ligand–metal-entering ligand angle of 75.6°. The structure of TS1 is consistent with data in literature, indicating that platinum planar square complexes undergo ligand substitution reactions via an associative interchange mechanism, passing through a pentacoordinate transition state [40].

The optimized product adduct PA1 geometry shows that the entering chloride ion has replaced the carboxylate ligand (Pt–Cl distance: 2.399 Å) and the leaving carboxylate group has moved away from the metal center (Pt–O distance: 3.733 Å) but is still interacting through a hydrogen bond with one ammino ligand (with a O–H distance of 1.77 Å), see Fig. 1c.

We then turned to the second activation step and considered the attack of a second chloride ion on the product of

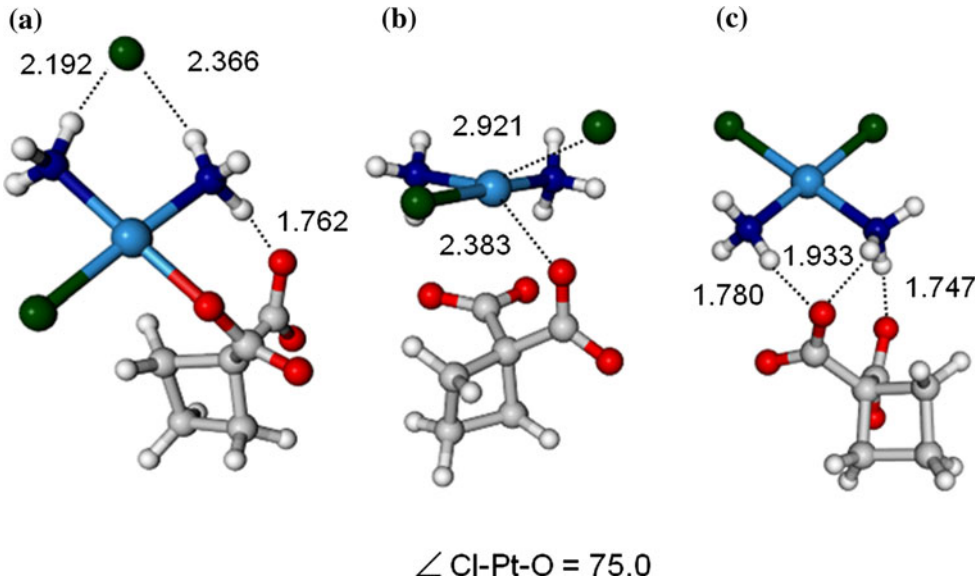

Fig. 2 Optimized geometries for the reactant adduct, RA2 (**a**), transition state, TS2 (**b**) and product adduct, PA2 (**c**) for the second activation step in neutral medium

the first step. The RA2 geometry (Fig. 2a) for this second step has a structure similar to that of PA1, with the uncoordinated carboxylate group hydrogen bound to one ammino ligand, and again sees the attacking chloride ion bridging, via hydrogen bonds, the ammino ligands, with Pt–Cl and Pt–O(leaving) distances of 4.287 and 2.053 Å, respectively, slightly larger than in the RA1 adduct, due to the different charge of the carboplatin fragment (neutral in the first step and negative in the second).

Figure 2b displays the optimized geometry for TS2 (imaginary frequency $= -125.7$ cm^{-1}): the entering chloride has approached the metal center with a Pt–Cl distance of 2.921 Å, again larger than for TS1, while the oxygen of the adjacent leaving carboxylate group has moved farther (Pt–O distance: 2.383 Å), with both oxygens of the free carboxylate group interacting, via hydrogen bond, with the ammino ligands. These distances, together with the calculated value of the Cl–Pt–O angle, 75.0°, indicate again an approximate trigonal bipyramidal geometry for this transition state. Moreover, the longer Pt–Cl and shorter Pt–O(malonate) bond distances suggest an earlier transition state with respect to the first activation step.

In the PA2 intermediate, the entering chloride has replaced the carboxylate ligand leading to cisplatin, with Pt–Cl and Pt–O(malonate) distances of 2.406 and 3.790 Å, respectively. The leaving malonate species is still bound to the complex through hydrogen bonds with the ammino ligands, see Fig. 2c.

3.1.2 Energy profiles

In Table 1, we report the reaction (RAn → PAn, $n = 1, 2$) and activation (RAn → TSn, $n = 1, 2$) enthalpies, free energies, and free solvation energies, calculated at B3LYP and LMP2 levels of theory, for the activation in neutral conditions. Two sets of data are given for the values in solution, those obtained from single-point calculations on the gas phase optimized geometries and those obtained upon optimization in solution phase.

The inclusion of the solvent generally reduces the activation enthalpy and free energies, while providing a smaller effect on the reaction enthalpies and free energies. Such a behavior is particularly remarkable for the first step and is probably due to the stabilization of the incipient carboxylate anion by the solvent.

A further geometry optimization in solution emphasizes the overall trend and leads to values of activation enthalpies and free energies in better agreement with experimental data. This result is consistent with a large body of theoretical calculations on biologically active metal-containing complexes, showing that optimization in solution improves the quantitative reproduction of the experimental activation and reaction energies [30], see for example [41].

Table 1 also shows that the energy barriers calculated at LMP2 level of theory are slightly larger than those calculated at B3LYP level, by ca. 4–6 kJ mol^{-1}. These differences are consistent with the well-known underestimation of the energy barriers at DFT level of theory [30, 31]. Therefore, only the LMP2 data will be discussed below.

From Table 1, it can be noted that the values of activation and reaction free energies are very close to the corresponding enthalpies (within 6 kJ mol^{-1}); therefore only free energy values will be discussed in the following, unless explicitly stated. Figure 3 displays the free energy profiles for the two activation steps using the results obtained from the optimization in solution at both levels of theory. The values are referred to the reagents infinitely

Table 1 Calculated enthalpy, free energy, and free solvation energy for the carboplatin activation in neutral medium

B3LYP						
	Gas phase[a]		Solution phase (single point)[b]		Solution phase (optimization)[c]	
	RA1 → TS1	RA1 → PA1	RA1 → TS1	RA1 → PA1	RA1 → TS1	RA1 → PA1
First step						
ΔH	236.8	116.8	171.9	87.9	132.8	43.7
ΔG	238.5	124.5	172.9	92.0	133.8	47.9
ΔΔGsolv			−64.8	−28.9	−135.2	−83.1
	Gas phase		Solution phase (single point)		Solution phase (optimization)	
	RA2 → TS2	RA2 → PA2	RA2 → TS2	RA2 → PA2	RA2 → TS2	RA2 → PA2
Second step						
ΔH	199.5	1.8	170.5	17.2	128.9	12.1
ΔG	202.5	3.0	172.1	17.9	130.5	12.8
ΔΔGsolv			−29.0	15.4	−86.2	4.5
LMP2						
	Gas phase[d]		Solution phase (single point)[e]		Solution phase (optimization)[f]	
	RA1 → TS1	RA1 → PA1	RA1 → TS1	RA1 → PA1	RA1 → TS1	RA1 → PA1
First step						
ΔH	263.8	123.2	195.2	85.8	137.0	42.3
ΔG	265.5	130.9	196.1	89.9	137.9	46.4
ΔΔGsolv			−68.6	−37.4	−155.6	−108.9
	Gas phase		Solution phase (single point)		Solution phase (optimization)	
	RA2 → TS2	RA2 → PA2	RA2 → TS2	RA2 → PA2	RA2 → TS2	RA2 → PA2
Second step						
ΔH	212.2	3.7	186.0	19.1	132.0	16.0
ΔG	215.2	5.0	187.6	19.8	133.6	16.7
ΔΔGsolv			−26.2	15.4	−87.1	4.7

Values in kJ mol^{-1}

[a] B3LYP/BS2//B3LYP/LACVP**

[b] PB/B3LYP/BS2//B3LYP/LACVP**

[c] PB/B3LYP/BS2//PB/B3LYP/LACVP**

[d] LMP2/BS2//B3LYP/LACVP**

[e] PB/LMP2/BS2//B3LYP/LACVP**

[f] PB/LMP2/BS2//PB/B3LYP/LACVP**

apart and explicitly report the free energy of the formation of adducts RA1, RA2, PA1 and PA2, and the final products P2($CBDCA^{2-}$) and cisplatin infinitely apart.

The formation of the adduct RA1 from carboplatin and Cl^- infinitely apart is an approximately thermoneutral process. The values of reaction enthalpy and free energy with respect to this adduct, 42 and 46 kJ mol^{-1}, respectively, indicate that the malonate ring opening by Cl^- is an endothermic and endergonic process. Activation enthalpy and free energies are also quite large (more than 135 kJ mol^{-1}), indicating a kinetically demanding process.

The second activation step, passing through the thermoneutral formation of the RA2 adduct, is also endothermic and endergonic–though to a lesser extent–with reaction free energy about 16 kJ mol^{-1}. The corresponding activation free energy, 134 kJ mol^{-1}, shows that also this step is kinetically demanding.

On the whole, the calculated values of the activation and reaction enthalpies and free energies for both steps suggest that the carboplatin activation process in neutral conditions is highly unfavorable both kinetically and thermodynamically. These results are in agreement with the experimental

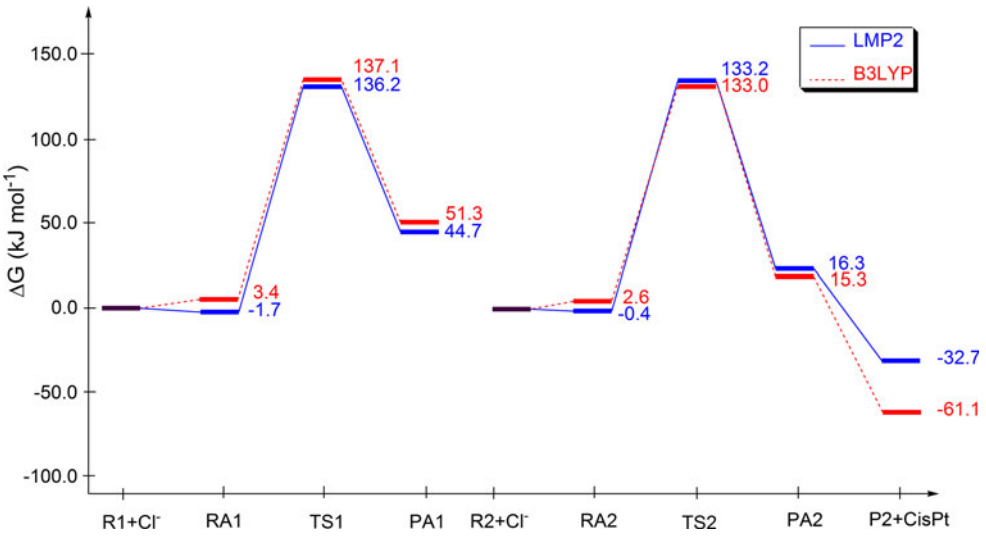

Fig. 3 Free energy profiles for the first (*left*) and second (*right*) activation step in neutral conditions

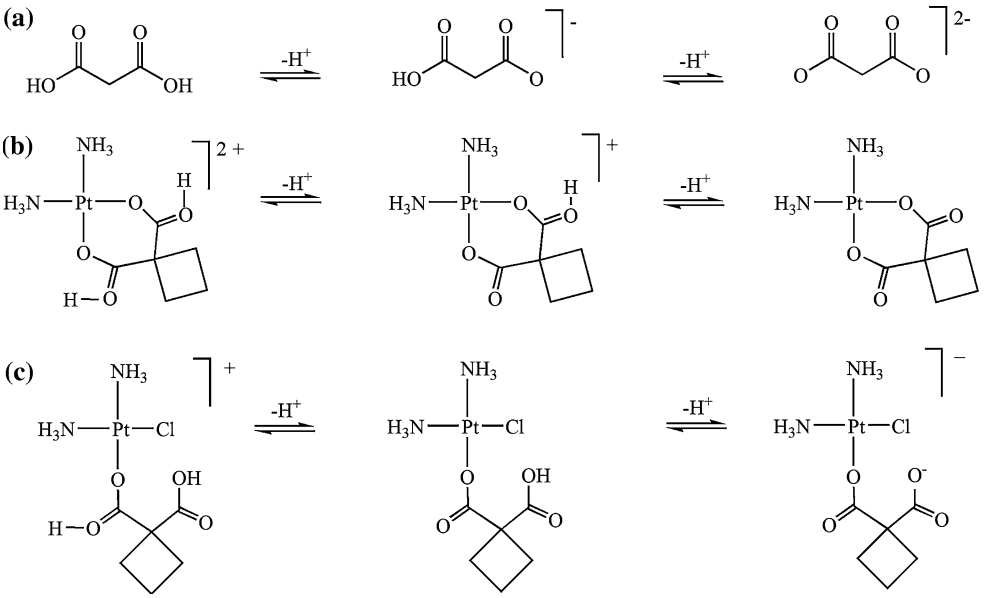

Scheme 2 Reaction schemes for the calculation of pK_a's for **a** malonic acid, **b** doubly protonated carboplatin, $[(NH_3)_2Pt(CBDCA)H_2]^{2+}$ and **c** $[(NH_3)_2PtCl(CBDCA)H]^{+}$

evidence [6, 7, 9], indicating that in such conditions, the displacement of the CBDCA group of carboplatin by the chloride ion occurs at a negligible rate at 25 °C. A temperature of 80 °C has to be reached for the reaction to proceed at an appreciable rate [6].

3.2 Activation in acidic medium

The acid-catalyzed activation reaction can be simulated assuming that the carboplatin complex undergoing the chloride ion attack has been previously protonated. Two plausible protonation sites are available for carboplatin, the carbonyl oxygen atoms of the CBDCA ligand, leading to $[(NH_3)_2Pt(CBDCA)H]^{+}$ and $[(NH_3)_2Pt(CBDCA)H_2]^{2+}$. In order to estimate at which pH values these sites begin to be protonated, we evaluated their absolute pK_a values. To test the reliability of our theoretical approach to reproduce the pK_a values for this kind of compounds, we calculated the pK_{a1} and pK_{a2} of malonic acid (see Scheme 2a), whose experimental values are 2.8 and 5.7 [42]. We calculated pK_a's of 1.4 and 5.3 that, although slightly underestimated, are in reasonably good agreement with the experimental values. The calculated pK_a's of −9.4 and −1.7, respectively, for $[(NH_3)_2Pt(CBDCA)H_2]^{2+}$ and $[(NH_3)_2Pt(CBDCA)H]^{+}$ (Scheme 2b) are lower than the corresponding ones for the malonic acid, as expected due to the coordination of the double positively charged Pt^{2+} metal ion, which makes the protonation process more difficult. In particular, these pK_a values, although probably slightly underestimated as those for malonic acid, indicate that the doubly protonated carboplatin is an extremely unstable structure, unlikely to exist even in strong acidic media. For

this reason, the first step in path 1c (Scheme 1) has been ruled out. The carboplatin monoprotonation, on the other hand, can occur in strong acidic condition, leading to significant concentration of $[(NH_3)_2Pt(CBDCA)H]^+$. However, although it has been shown that the microenvironment in many types of tumor is slightly acid, with pH in the range from 5.8 to 7.2 [43, 44], these conditions are not sufficient to ensure carboplatin protonation, and neutral carboplatin is the main species undergoing the Cl^- attack.

On the other hand, the monoprotonated $[(NH_3)_2Pt(CBDCA)H]^+$ species can be used to simulate the activation reaction taking place in strong acidic media (see Scheme 3b).

We should also take into account that the product of the first activation step in neutral conditions, $[(NH_3)_2PtCl(CBDCA)]^-$, bears a carboxylate moiety and is therefore expected to be significantly more basic than carboplatin itself. Indeed, for this monochlorinated species, we calculated pK_a values of -1.9 and $+6.2$ for $[(NH_3)_2PtCl(CBDCA)H_2]^+$ and $[(NH_3)_2PtCl(CBDCA)H]$, respectively (Scheme 2c). These values indicate that while the doubly protonated open ring compound could only be involved in very strong acidic conditions (pH < 0), the monoprotonated $[(NH_3)_2PtCl(CBDCA)H]$ species may have a significant concentration already at pH slightly below 7, conditions which can be found in the tumor environment.

Scheme 3 summarizes the pathways that we took into account to simulate the two-step activation process in weak acidic medium (Scheme 3a), similar to that of the tumor microenvironment, and in strong acidic condition (Scheme 3b), as those employed in the experimental in vitro reaction using concentrated HCl, which has been found to lead to cisplatin.

3.2.1 *Activation in weak acidic medium*

3.2.1.1 Geometry structures As stated before, the first step of the activation reaction taking place at weak acidic condition is essentially the same as described for the reaction in neutral condition.

The adduct between the monoprotonated $[(NH_3)_2PtCl(CBDCA)H]$ product of the first step and the chloride ion was instead taken as the reactant adduct, RA2, for the second activation step. The optimized geometry of RA2 (Fig. 4a) shows the attacking chloride ion simultaneously interacting with two ammino hydrogens and the protonated carboxylate function. The Pt–Cl(entering) and Pt–O distances are 3.990 and 2.067 Å, respectively.

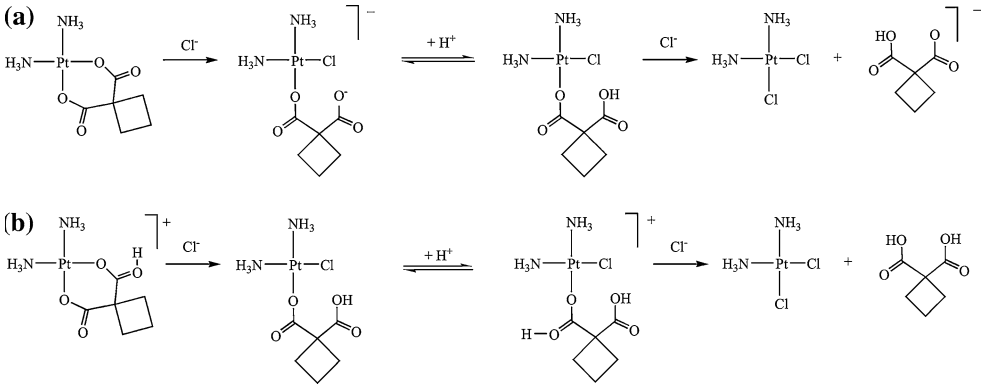

Scheme 3 Reaction schemes for the activation of carboplatin in acidic media: **a** weak acid conditions and **b** strong acid conditions

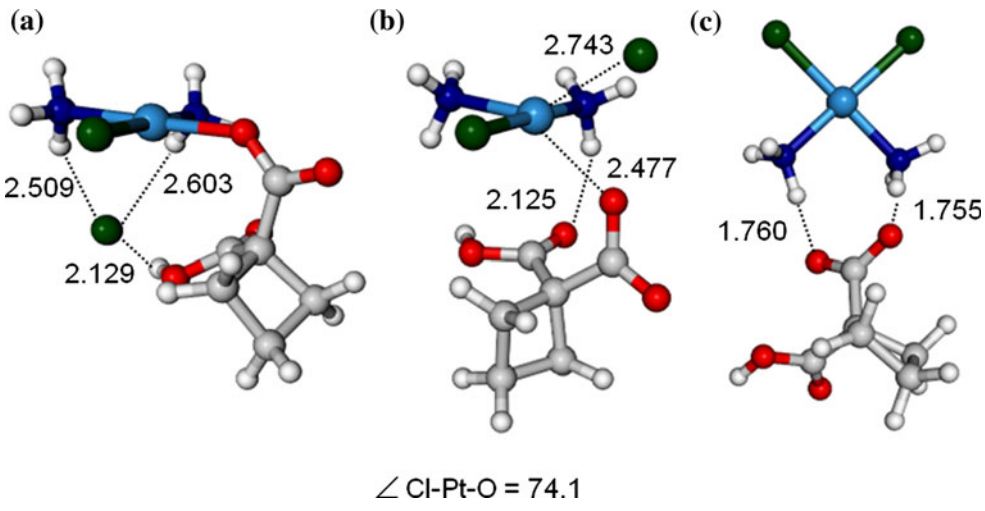

Fig. 4 Optimized geometries for the reactant adduct, RA2 (**a**), transition state, TS2 (**b**) and product adduct, PA2 (**c**) for the second activation step in weak acidic medium

The transition state TS2 (Fig. 4b, with an imaginary frequency of -141.8 cm^{-1}) also shows a trigonal bipyramidal structure, with slightly larger Pt–O and slightly shorter Pt–Cl distances than those corresponding to TS2 in water, probably due to the neutral character of $[(NH_3)_2PtCl(CBDCA)H]$ with respect to the anionic $[(NH_3)_2PtCl(CBDCA)]^-$.

In the product adduct (Fig. 3c), PA2, the oxygens of the unprotonated carboxylate function tightly interact with the ammino hydrogens, with Pt–Cl and Pt–O distances of 2.399 and 4.011 Å, respectively.

3.2.1.2 Energy profiles The reaction and activation enthalpies, free energies, and free solvation energies are given in Table 2, whereas the energy profile for the activation in weak acidic medium is reported in Fig. 5.

The high activation free energy and the endergonicity of the first step, already discussed in the preceding section, suggest that the activation of carboplatin is unlikely to occur in weak acidic conditions at physiological temperature, as it happens in neutral medium. However, for the sake of completeness, the second step is described in detail in the following.

The activation of $[(NH_3)_2PtCl(CBDCA)H]$ leading to the final cisplatin and hydrogen malonate is approximately thermoneutral, with the formation of the reactant adduct, RA2, slightly endergonic, by 5 kJ mol^{-1}. Activation free energies are comparable to those evaluated for the second step of the reaction in neutral conditions, about 134 kJ mol^{-1}, indicating that this process is also kinetically unfavored at 25 °C.

3.2.2 Activation in strong acidic medium

As described before, activation in strong acidic conditions will be simulated according to Scheme 3b, the first step consisting of the attack of Cl^- to the monoprotonated carboplatin $[(NH_3)_2Pt(CBDCA)H]^+$ and the second of the attack of the chloride to the doubly protonated species $[(NH_3)_2PtCl(CBDCA)H_2]^+$.

3.2.2.1 Geometry structures The optimized reactants adduct RA1 geometry shows a hydrogen bond pattern different from that observed for the neutral carboplatin, with the attacking chloride bonded via hydrogen bonds to an ammino ligand and to the protonated carboxylate ligand, see Fig. 6a. The interaction distances are shorter than those calculated for the neutral complex, and as a result, Cl^- is closer to the metal center (with a Pt–Cl distance of 4.143 Å).

The transition state TS1 (imaginary frequency = -152.1 cm^{-1}) has a trigonal bipyramidal structure similar to the TS1 for the corresponding neutral process, the main difference being the role of the leaving oxygen that is protonated and interacts, via hydrogen bond, with the attacking chloride, see Fig. 6b. Pt–Cl and Pt–O(malonate) distances are 2.905 and 2.489 Å, respectively, whereas the leaving ligand–metal-entering ligand angle is 70.1°. The hydrogen bond interaction of the Cl^- ion with the protonated carboxylate is responsible for the Pt–Cl distance longer than in the neutral complex, whereas the Pt–O distance remains substantially unvaried.

The overall coordination geometry around the metal center for the product intermediate, PA1, is also very close to that observed for the product of the first step of the activation in neutral conditions, see Fig. 6c, with Pt–Cl and Pt–O(malonate) distances of 2.386 and 3.447 Å, respectively, and a slightly larger hydrogen bond distance due to the neutral charge of the involved carboxylate group that is protonated in acidic medium.

The adduct formed by the doubly protonated $[(NH_3)_2PtCl(CBDCA)H_2]^+$ and the chloride ion, RA2, shows an optimized geometry (Fig. 7a) very close to the corresponding species for the activation in neutral solution with the attacking chloride ion bridging, via hydrogen bonds, the ammino ligands, with interaction distances, Pt–Cl: 4.261 Å and Pt–O: 2.143 Å.

The transition state TS2 (Fig. 7b, with an imaginary frequency of -138.8 cm^{-1}) shows again a trigonal bipyramidal structure with Pt–Cl(entering) and Pt–O(leaving) distances of, respectively, 2.878 and 2.474 Å, slightly shorter than those for the corresponding first step.

In the final neutral product PA2, the leaving malonate species is still closely bound to the complex (cisplatin) through hydrogen bonds to the ammino ligands; the chloride ligand distance, 2.389 Å, is very similar to that for the first step, whereas the released malonato moiety is much farther than in the first step (Pt–O distance 4.105 Å), see Fig. 7c.

3.2.2.2 Energy profiles The reaction and activation enthalpies, free energies, and free solvation energies are given in Table 3, whereas the energy profile for the activation in strong acidic medium is reported in Fig. 8.

At variance with the results found for neutral conditions, the reactant adduct, although significantly more stable than the infinitely separated reagents in gas phase, becomes unstable when the solvent effect is included, by ca. 60 kJ mol^{-1}, probably due to the loss of solvation energy when the two charged reactants are bound together. The transition state TS1 is ca. 55 kJ mol^{-1} in free energy above this adduct and leads to a product adduct, PA1, close in free energy to initial reactants infinitely apart. The overall process results essentially thermoneutral with a total activation free energy of 113.9 kJ mol^{-1} indicating that the first step in strong acid is kinetically more favored than in neutral and weak acidic media.

Table 2 Calculated enthalpy, free energy, and solvation free energy for the carboplatin activation in weak acidic medium

B3LYP						
	Gas phase[a]		Solution phase (single point)[b]		Solution phase (optimization)[c]	
	RA1 → TS1	RA1 → PA1	RA1 → TS1	RA1 → PA1	RA1 → TS1	RA1 → PA1
First step						
ΔH	236.8	116.8	171.9	87.9	132.8	43.7
ΔG	238.5	124.5	172.9	92.0	133.8	47.9
ΔΔGsolv			−64.8	−28.9	−135.2	−83.1
	Gas phase		Solution phase (single point)		Solution phase (optimization)	
	RA2 → TS2	RA2 → PA2	RA2 → TS2	RA2 → PA2	RA2 → TS2	RA2 → PA2
Second step						
ΔH	216.0	−21.1	155.1	−7.3	118.7	−8.4
ΔG	209.3	−26.9	151.5	−10.5	115.1	−11.5
ΔΔGsolv			−60.9	13.8	−104.9	38.2
LMP2						
	Gas phase[d]		Solution phase (single point)[e]		Solution phase (optimization)[f]	
	RA1 → TS1	RA1 → PA1	RA1 → TS1	RA1 → PA1	RA1 → TS1	RA1 → PA1
First step						
ΔH	263.8	123.2	195.2	85.8	137.0	42.3
ΔG	265.5	130.9	196.1	89.9	137.9	46.4
ΔΔGsolv			−68.6	−37.4	−155.6	−108.9
	Gas phase		Solution phase (single point)		Solution phase (optimization)	
	RA2 → TS2	RA2 → PA2	RA2 → TS2	RA2 → PA2	RA2 → TS2	RA2 → PA2
Second step						
ΔH	239.4	−7.5	163.4	−4.8	128.6	−1.7
ΔG	232.7	−13.3	159.8	−7.9	125.0	−4.8
ΔΔGsolv			−76.0	2.7	−112.6	34.1

Values in kJ mol^{-1}

[a] B3LYP/BS2//B3LYP/LACVP**

[b] PB/B3LYP/BS2//B3LYP/LACVP**

[c] PB/B3LYP/BS2//PB/B3LYP/LACVP**

[d] LMP2/BS2//B3LYP/LACVP**

[e] PB/LMP2/BS2//B3LYP/LACVP**

[f] PB/LMP2/BS2//PB/B3LYP/LACVP**

The second activation step in such conditions can also occur easily. Indeed, the endothermic formation of the reactant adduct, RA2, is followed by the formation of TS2, which only requires 90.6 kJ mol^{-1} in free energy (from the reactants infinitely apart) to give a stable product adduct at −13.1 kJ mol^{-1}. The complete separation of the final products, cisplatin and malonic acid, leads to a further stabilization, so that the whole process is very exothermic ($\Delta H = -35.5$ kJ mol^{-1}), indicating that the second step is much more favored, both kinetically and thermodynamically, in strong acidic media than in neutral or weak acidic conditions.

Furthermore, a rapid second step can account for a fast removal of the products of the first step thermoneutral process, shifting this equilibrium toward the production of $[(NH_3)_2PtCl(CBDCA)H_2]^+$.

On the whole, these results suggest that the activation of carboplatin in strongly acidic medium is a thermodynamically favored process which can occur rather rapidly. This conclusion agrees well with the experimental evidences,

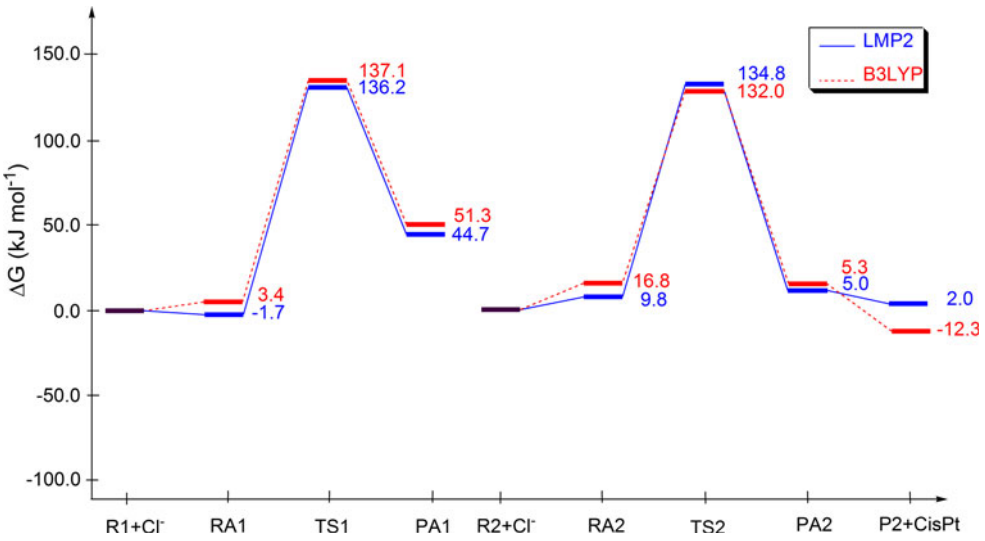

Fig. 5 Free energy profiles for the first (*left*) and second (*right*) activation step in weak acidic medium

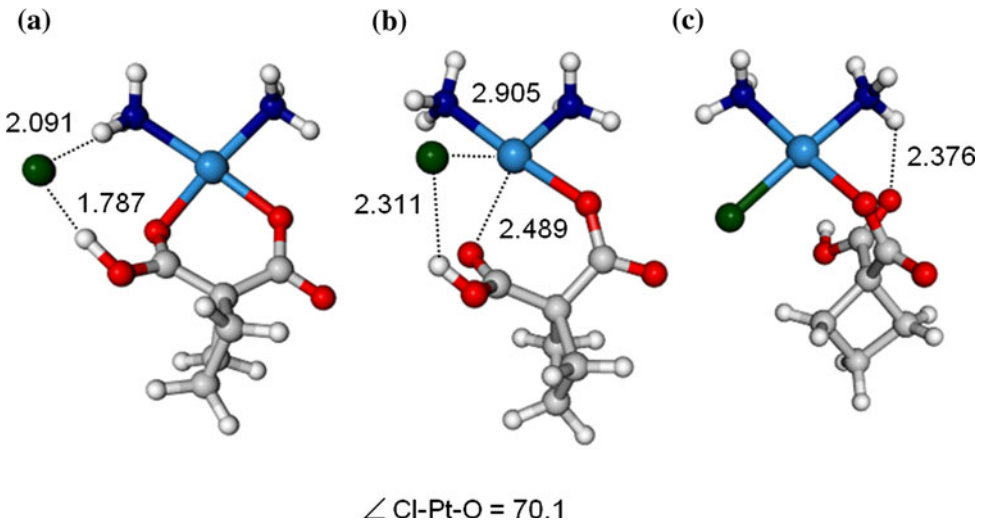

Fig. 6 Optimized geometries for the reactant adduct, RA1 (**a**), transition state, TS1 (**b**) and product adduct, PA1 (**c**), for the first activation step in strong acidic medium

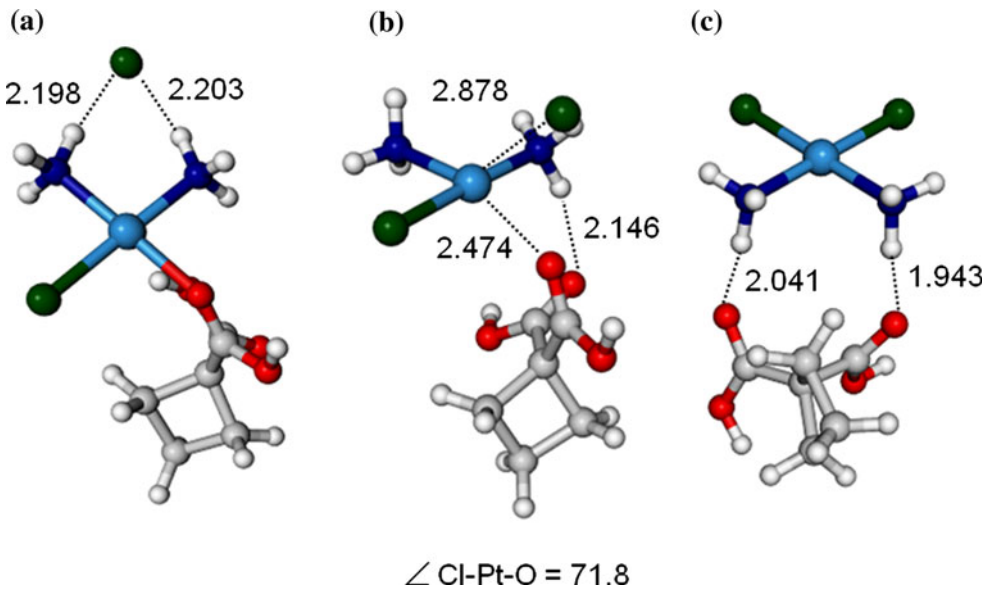

Fig. 7 Optimized geometries for the reactant adduct, RA2 (**a**), transition state, TS2 (**b**) and product adduct, PA2 (**c**), for the second activation step in strong acidic medium

Table 3 Calculated enthalpy, free energy, and solvation free energy for the carboplatin activation in strong acidic medium

B3LYP						
	Gas phase[a]		Solution phase (single point)[b]		Solution phase (optimization)[c]	
	RA1 → TS1	RA1 → PA1	RA1 → TS1	RA1 → PA1	RA1 → TS1	RA1 → PA1
First step						
ΔH	76.8	−26.2	78.3	−21.9	55.9	−36.7
ΔG	79.6	−31.1	79.8	−24.6	57.4	−39.4
ΔΔGsolv			1.5	4.2	−45.2	−35.9
	Gas phase		Solution phase (single point)		Solution phase (optimization)	
	RA2 → TS2	RA2 → PA2	RA2 → TS2	RA2 → PA2	RA2 → TS2	RA2 → PA2
Second step						
ΔH	100.3	−47.8	64.8	−23.0	68.2	−35.6
ΔG	94.2	−50.2	61.6	−24.3	65.0	−35.8
ΔΔGsolv			−35.4	24.8	−29.7	0.1
LMP2						
	Gas phase[d]		Solution phase (single point)[e]		Solution phase (optimization)[f]	
	RA1 → TS1	RA1 → PA1	RA1 → TS1	RA1 → PA1	RA1 → TS1	RA1 → PA1
First step						
ΔH	73.2	−46.0	76.3	−46.4	50.3	−57.5
ΔG	76.0	−50.8	77.8	−49.0	51.8	−60.2
ΔΔGsolv			3.1	−0.4	−46.1	−29.7
	Gas phase		Solution phase (single point)		Solution phase (optimization)	
	RA2 → TS2	RA2 → PA2	RA2 → TS2	RA2 → PA2	RA2 → TS2	RA2 → PA2
Second step						
ΔH	61.1	−89.8	65.8	−35.5	62.6	−43.1
ΔG	55.0	−92.2	62.5	−36.8	59.3	−44.4
ΔΔGsolv			4.7	54.4	−26.5	−0.5

Values in kJ mol^{-1}

[a] B3LYP/BS2//B3LYP/LACVP**

[b] PB/B3LYP/BS2//B3LYP/LACVP**

[c] PB/B3LYP/BS2//PB/B3LYP/LACVP**

[d] LMP2/BS2//B3LYP/LACVP**

[e] PB/LMP2/BS2//B3LYP/LACVP**

[f] PB/LMP2/BS2//PB/B3LYP/LACVP**

indicating that carboplatin gives yellow crystals of cisplatin in hydrochloric acid solution at 25 and at 37 °C [6, 7].

4 Final remarks

We performed an ab initio study to investigate the mechanism of carboplatin activation by chloride ions in different pH conditions. Both DFT- and LMP2-based methods were used to calculate reaction and activation enthalpies and free energies, with similar results, although LMP2 barriers are consistently slightly higher. The effect of optimization in solution was also taken into account and shown to play a significant role in the determination of more reliable values.

In conclusion, our calculations indicate that the process in neutral conditions, or in weak acidic conditions, such as those occurring in the hypoxic tumor environment, is very unlikely to occur at room or at physiological temperature, suggesting that substitution by chloride ions does not

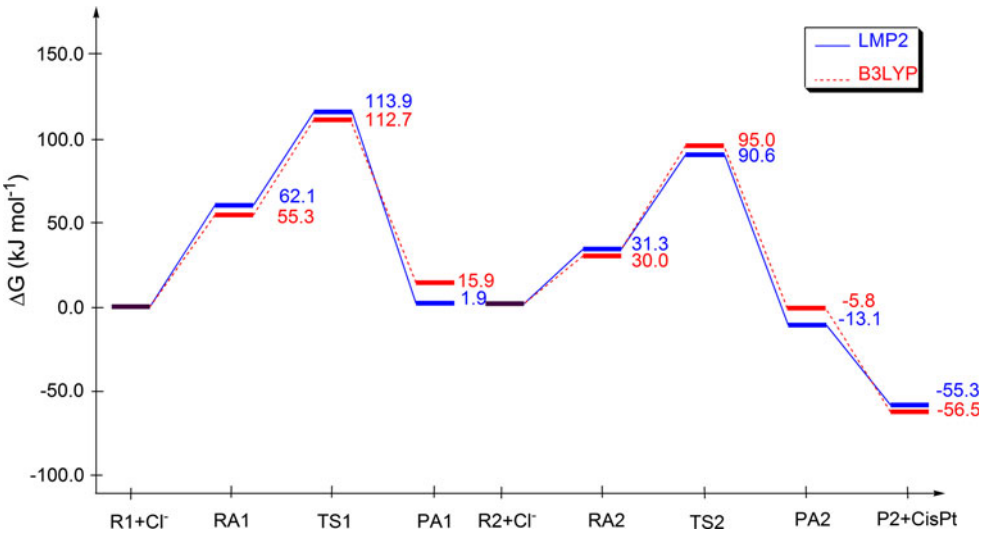

Fig. 8 Free energy profiles for the first (*left*) and second (*right*) activation step in strong acidic medium

represent a viable path for carboplatin activation in vivo and that enzymatic degradation or nucleophiles stronger than chloride are required to convert carboplatin to a dichloro species.

On the other hand, our results confirm that in strong acidic conditions, the reaction proceeds at significant rate at 25 °C, with both steps remarkably exergonic, leading to the rapid and irreversible formation of cisplatin.

Acknowledgments The authors would like to thank one of the reviewers for suggestions. Funding from University "G. d'Annunzio" is gratefully acknowledged.

References

1. Rosenberg B, Van Camp L, Trosko JE, Mansour VH (1969) Nature 222:385–387
2. Jamieson ER, Lippard SJ (1999) Chem Rev 99:2467–2498
3. Wang D, Lippard SJ (2005) Nature Rev Drug Discuss 4:307–320
4. Wong E, Giandomenico CM (1999) Chem Rev 99:2511–2534
5. Boulikas T, Vougiouka M (2003) Oncol Rep 10:1663–1682
6. Canovese L, Cattalini L, Chessa G, Tobe ML (1988) J Chem Soc Dalton Trans 2135–2140
7. Frey U, Ranford JD, Sadler PJ (1993) Inorg Chem 32:1333–1340
8. Barnham KJ, Djuran MI, Murdoch PS, Ranford JD, Sadler PJ (1996) Inorg Chem 35:1065–1072
9. Allsopp MA, Sewell J, Rowland CG, Riley CM, Schowen RL (1991) Int J Pharm 69:197–210
10. Calvert H, Judson I, van der Vijgh WJ (1993) Cancer Surv 17:189–217
11. Hay RW, Miller S (1998) Polyhedron 17:2337–2343
12. Burda JV, Zeizinger M, Leszczynski J (2005) J Comput Chem 26:907–914
13. Pavelka M, Lucas MFA, Russo N (2007) Chem Eur J 13:10108–10116
14. Lucas MFA, Pavelka M, Alberto ME, Russo N (2009) J Phys Chem B 113:831–838
15. Alberto ME, Lucas MFA, Pavelka M, Russo N (2009) J Phys Chem B 113:14473–14479
16. Alberto ME, Lucas MFA, Pavelka M, Russo N (2008) J Phys Chem B 112:10765–10768
17. Jaguar (2008) version 7.5, Schrödinger, LLC, New York
18. Becke AD (1993) J Chem Phys 98:5648–5652
19. Becke AD (1988) Phys Rev A 38:3098–3100
20. Niu S, Hall BM (2000) Chem Rev 100:353–405
21. Nielsen RJ, Keith JM, Stoltz BM, Goddard WA III (2004) J Am Chem Soc 126 :7967–7974
22. Sæbø S, Tong W, Pulay P (1993) J Chem Phys 98:2170–2175
23. Hay PJ, Wadt WR (1985) J Chem Phys 82:299–310
24. Hariharan PC, Pople JA (1972) Chem Phys Lett 16:217–219
25. Zhao Y, Truhlar DG (2008) Theor Chem Acc 120:215–241
26. Zhao Y, Truhlar DG (2005) Acc Chem Res 41:157–167
27. Sousa SF, Fernandes PA, Ramos MJ (2003) J Phys Chem A 111:10439–10452
28. Tannor DJ, Marten B, Murphy R, Friesner RA, Sitkoff D, Nicholls A, Ringnalda M, Goddard WA III, Honig B (1994) J Am ChemSoc 116:11875–11882
29. Dunning TH Jr (1989) J Chem Phys 90:1007–1023
30. Zheng J, Zhao Y, Truhlar DG (2007) J Chem Theory Comput 3:569–582
31. Rotzinger FP (2005) J Phys Chem B 109:1510–1527
32. Werz DH (1980) J Am Chem Soc 102:5316–5322
33. Cooper J, Ziegler T (2002) Organometallics 41:6614–6622
34. Lau JKC, Deubel DV (2006) J Chem Theory Comp 2:103–106
35. Nielsen AhlquistM, Periona RA RJ, Goddard WA III (2009) J Am Chem Soc 131:17110–17115
36. Zhu H, Ziegler T (2009) Organometallics 28:2773–2777
37. Bercaw JE, Chen GS, Labinger JA, Lin BL (2010) Organometallics 29:4354–4359
38. Beagley B, Cruickshank DWJ, McAuliffe CA, Pritchard RG, Zaki AM, Beddoes RL, Cernik RJ, Mills OS (1985) J Mol Struct 130:97–102
39. Neidle S, Ismail IM, Sadler PJ (1980) J Inorg Biochem 13:205–212
40. Rotzinger FP (2005) Chem Rev 105 :2003–2037 and references therein
41. Bešker N, Coletti C, Marrone A, Re N (2008) J Phys Chem B 112:3871–3875
42. Petrucci RH, Harwood WS, Herring G (2002) General chemistry: principles and modern applications, 8th edn. Prentice Hall Inc, NJ
43. Wike-Hooley JL, Haveman J, Reinhold JS (1984) Radiother Oncol 2:343–366
44. Tannock IF, Rotin D (1989) Cancer Res 49:4373–4384